Available online at www.sciencedirect.com

SciVerse ScienceDirect

Ceramics International 39 (2013) 2037–2043

CERAMICS INTERNATIONAL

www.elsevier.com/locate/ceramint

Porous Gd-doped ceria barrier layer on solid oxide fuel cell with $Sm_{0.5}Sr_{0.5}CoO_{3-\delta}$ Cathodes

Young Min Park[a], Haekyoung Kim[b,*]

[a]Fuel Cell Project, Research Institute of Industrial Science and Technology, Pohang 790-330, Korea
[b]School of Materials Science & Engineering, Yeungnam University, Gyeongsan 712-749, Korea

Received 6 August 2012; received in revised form 13 August 2012; accepted 18 August 2012
Available online 23 August 2012

Abstract

Cobaltite based perovskites, such as $Sm_{0.5}Sr_{0.5}CoO_{3-\delta}$ (SSC), are attractive as a cathode for solid oxide fuel cell (SOFC) due to their high electrochemical activity and electrical conductivity. In this study, nano-sized SSC powders were synthesized by a complex method. To prevent reactions between cathode and an yttria-stabilized zirconia (YSZ) electrolyte, we propose a Gd-doped ceria (GDC) porous barrier layer and formed barrier layers, screen-printed to 5, 10, and 15 μm thicknesses. The performance of SOFCs without a GDC layer decrease by 23% from 0.78 Wcm^{-2} to 0.6 Wcm^{-2} after 12 h of operation at 780 °C. A SOFC with a screen-printed GDC of 5 μm shows a performance decrease of only 4% from 0.75 Wcm^{-2} to 0.72 Wcm^{-2} after 12 h of operation at 780 °C. Fuel cell performance decreases with decreasing thickness of the porous GDC layer, which may result from the lowered SSC active area due to its reaction with the YSZ electrolyte. The increase in ohmic resistance due to a thicker porous GDC layer is mitigated by a decrease in ohmic resistance due to reduced reaction between the SSC and YSZ. To use SSC in SOFCs, a barrier layer should be applied to obtain grater fuel cell performance and stability.
© 2012 Elsevier Ltd and Techna Group S.r.l. All rights reserved.

Keywords: Solid oxide fuel cell; Anode supported cell; Barrier layer; $Sm_{0.5}Sr_{0.5}CoO_{3-\delta}$

1. Introduction

Solid oxide fuel cells (SOFCs) are considered as an efficient and environmental friendly power generation system for power plants and distributed power. Their high operating temperature limits the selection of materials and components, concerning long-term stability, motivating a reduction in SOFC operation temperature. However, the ohmic and polarization resistances increase when the operation temperature decreases, thus decreasing fuel cell performance. The $La_{1-x}Sr_xMnO_3$ (LSM)-based cathode is a commonly used cathode material for high temperature SOFCs, but it performs poorly because of sluggish oxygen reduction reaction (ORR) kinetics, causing the cell to have a low current drawing capacity when the operating temperature of a single SOFC is below 800 °C. Hence, considerable efforts are being made to develop a new class of perovskite-based cathode materials for SOFCs that have mixed ionic and electronic conductivity with high electro-catalytic activity for oxygen reduction at relatively lower operating temperature (700–800 °C) [1–11]. Amongst these, cobaltite based perovskites such as $La_{0.5}Sr_{0.5}CoO_{3-\delta}$ (LSC), $Sm_{0.5}Sr_{0.5}CoO_{3-\delta}$ (SSC), $La_{0.5}Sr_{0.5}Co_{0.2}Fe_{0.8}O_{3-\delta}$ (LSCF), and $Ba_{0.5}Sr_{0.5}Co_{0.8}Fe_{0.2}O_{3-\delta}$ (BSCF), are attractive due to their high electrochemical activity and electrical conductivity [12–19]. A BSCF cathode exhibits very low polarization resistance due to its high oxygen diffusion coefficient and yields maximum power density at low temperature [20]. However, its large thermal expansion coefficient and low electrical conductivity result in mismatch with the electrolyte, thus limiting cell performance [21]. LSC possesses high electronic and oxygen ion conductivity over a wide temperature range, but it also has a large thermal expansion coefficient [22]. Although doping Co-site with Fe^{3+} (LSCF) can reduce the thermal expansion coefficient, the Fe^{3+} doping decreases LSC ionic conductivity [23]. $Sm_{1-x}Sr_xCoO_{3-\delta}$ compounds show higher ionic conductivity than $La_{1-x}Sr_xCoO_{3-\delta}$ [13,24,25], exhibiting better electronic conductivity

*Corresponding author. Tel.: +82 53 810 2536; fax: +82 53 810 4628.
E-mail address: hkkim@ynu.ac.kr (H. Kim).

0272-8842/$ - see front matter © 2012 Elsevier Ltd and Techna Group S.r.l. All rights reserved.
http://dx.doi.org/10.1016/j.ceramint.2012.08.056

than that of pure BSCF [26], and are good catalysts for oxygen reduction [27]. Ishihara et al. [28] and Fukunaga et al. [24] also reported that the overpotential of dense SSC film is lower than that of dense LSC film under the same condition and that the oxygen adsorption–desorption rate is one-order-magnitude higher than that of LSC. However, the disadvantages of SSC are its large thermal expansion coefficient and high reactivity with YSZ electrolyte at 900 °C or higher [25].

A dense or porous interlayer such as GDC and SDC has been used as an interlayer to reduce mismatch and prevent reactions between the cathode and YSZ electrolyte [29,30]. A thinner interlayer is preferred to prevent ohmic resistance increase, hence complex and expensive processes such as ADM (aerosol deposition method), physical vapor deposition, and pulsed laser deposition (PLD) are used to fabricate the interlayer [31,32]. However, the thickness of the porous interlayer has rarely been studied. In this study, we synthesized a cathode material of $Sm_{0.5}Sr_{0.5}CoO_{3-\delta}$ (SSC) using a complex method and investigated its thermal, physical, and chemical properties. SSC was applied as the cathode in anode-supported SOFCs with and without barrier layers. We will discuss the performance and stability of SOFCs with an YSZ electrolyte as related to the thicknesses of the porous GDC barrier layer.

2. Experiment

Starting materials used included $Sm(NO_3)_3 \cdot 6H_2O$ (4.440 g, 0.01 mol), $Sr(NO_3)_2$ (2.116g, 0.01 mol) and $Co(NO_3)_2 \cdot 6H_2O$ (5.821 g, 0.02 mol) all in analytical grades. They were dissolved in 100 ml of deionized water to prepare a homogeneous nitrate solution. Then, ethylenediaminetetraacetic acid (EDTA, 5.845 g, 0.04 mol) powders and citric acid (7.645 g, 0.02 mol) were added for chelating into a homogeneous nitrate solution. The solution was heated in a water bath at 70 °C. After obtaining a clear solution, the mixture was continuously heated to evaporate the water until the magnetic bar stopped rotating. The remaining mixture was dried at 80 °C in a vacuum oven overnight to remove residual water. The dried powders were crushed and calcined at 500–900 °C to form a perovskite phase removing all organic compounds. Thermogravimetric analysis (TGA) was carried out with crushed powders from room temperature to 1000 °C in air at a heating rate of 3 °C min^{-1} using a Shimadzu TA-50 Thermal Analyzer to investigate the thermal behavior. The calcined powders were characterized by means of X-ray diffraction and scanning electron microscopy (SEM) to observe their phases and morphologies. We investigated the chemical stability of SSC, YSZ, and GDC by mixing the powders in 50:50 wt% ratio. The mixed powder was pressed into pellets of 2 cm diameter and was heated to 600–900 °C. The stabilities of SSC, YSZ, and GDC, were analyzed and characterized with X-ray diffraction.

To characterize fuel cell performance, anode-supported cells (ASC), which consist of 900 μm Ni-YSZ as a support layer, 20 μm Ni-YSZ as an anode functional layer (AFL), and 10 μm YSZ as an electrolyte, were fabricated using tape casting and co-firing at 1370 °C. The anode-supported cells were cut into circles with diameters of 2.6 cm from a 25 cm × 25 cm plate. To fabricate a GDC barrier layer, GDC powder was prepared by a complex method with 0.1 mol $Gd(NO_3)_3 \cdot 6H_2O$, 0.9 mol $Ce(NO_3)_3 \cdot 6H_2O$, and 1 mol of citric acid. The GDC powder was calcinated at 800 °C for 3 h and then mixed with organic binder solution of ethyl cellulose, di-ethylene glycol butyl ether, and α-terpinol. GDC pastes were screen-printed onto a Ni-YSZ/YSZ anode-supported cell and then sintered at 1100 °C for 3 h. To enhance the sinterability, 1 mol % of Co_3O_4 was added to the GDC paste. The thicknesses of the GDC barrier layer were 5, 10, and 15 μm, which were controlled by screen-printing times. SSC pastes were prepared from synthesized SSC powders with 50 wt% organic binder solution and screen-printed on a Ni-YSZ/YSZ/GDC anode-supported cell. The cathodes were sintered at 800 °C for 3 h. The active cathode area was 0.785 cm^2. SOFC without a barrier layer was also fabricated with SSC, and compared with SOFCs with a barrier layer. SOFCs without a barrier layer were sintered at 600 °C after screen-printing of the SSC paste to prevent reaction between the SSC and YSZ.

The fabricated cells were assembled and sealed with Ceramabond 571 from AREMCO in a jig to measure current–voltage characteristic and impedances. Pt paste and mesh were used for current collection. The SOFCs were heated and anode reduction was performed with 300 cc min^{-1} of 97% H_2 – 3% H_2O for 3 h. Fuel cell performance was measured at each temperature with 300 cc min^{-1} of 97% H_2 – 3% H_2O and 1000 cc min^{-1} of air. The impedances were measured with a WEIS system from Wonnatech. The impedance spectra were obtained in the frequency range of 100 kHz to 0.1 Hz with applied AC voltage amplitude of 100 mV at each temperature and open circuit voltage. After electrochemical measurements, the SOFC microstructures were characterized with scanning electron microscopy of JSM-6480 LV.

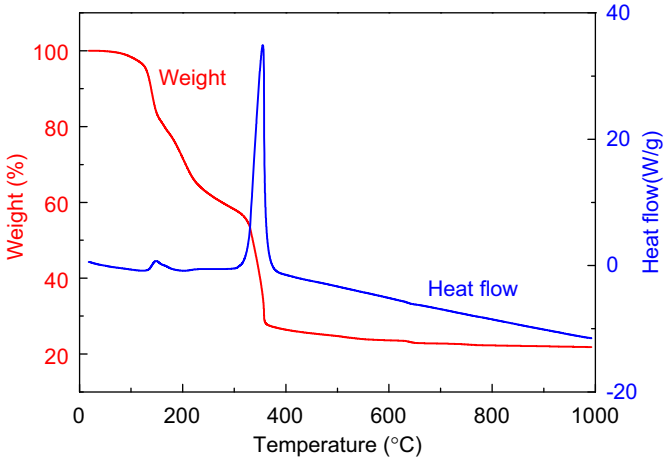

Fig. 1. Thermogravity curves of crushed SSC powders.

3. Results and discussion

The thermal analysis curves of the crushed powders are presented in Fig. 1. Significant weight losses were observed at ~175 °C and 350 °C due to water removal and decomposition of organic compounds such as citric acid and EDTA. Above 400 °C no significant weight loss was observed, and the heat flows for phase formation were characterized. From the XRD analysis, shown in Fig. 2, SSC perovskite peaks appear at 600 °C, and become sharper and narrower as the calcination temperature increases. The morphologies of SSC powder calcined at various temperatures are shown in Fig. 3.

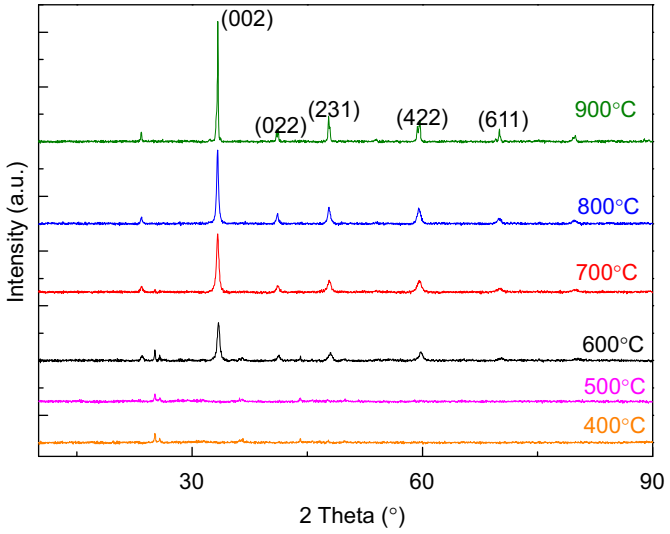

Fig. 2. XRD spectra of SSC powders calcined at various temperatures.

Fig. 3(a) and (b) show the sheets of small particles, and agglomeration is easily observed in Fig. 3(d). Fig. 3(b) shows particle sizes less than 100 nm. The smaller particles have a large surface area, resulting in higher catalytic performance. The powder calcined at 700 °C was used to characterize the fuel cell performances.

In SOFCs, the cathode needs to be chemically stable with the electrolyte. To measure the stability, pellets of SSC with YSZ were heat treated at various temperatures. As shown in Fig. 4(a), the second phase peaks, such as $SrZrO_3$ and $Sm_3Zr_2O_7$, appeared in the sample heat treated at 800 °C, and with increasing temperature the peaks become sharper and stronger [25]. We observe that SSC is stable with YSZ under 800 °C. In Tu's work, they reported that the reaction started at 900 °C [25]. Smaller particle size may enhance SSC reactivity with YSZ. A barrier layer, such as GDC, is therefore needed to prevent reactions between SSC and YSZ [5–8,18,24,25,29–33]. The stability of SSC with a GDC layer is shown in the XRD spectra of Fig. 4(b). SSC with a GDC layer is stable below 900 °C; a high enough temperature for SOFC operation. In this study, the stability of SSC with a GDC layer is confirmed and GDC is proposed as a barrier layer for SSC.

To study the effects of SSC reactions with YSZ in terms of electrical properties, porous pellets of SSC and YSZ were heat-treated at 600 °C. The SEM images of the pellet are shown in Fig. 5, which shows that the morphology of a porous pellet is similar to the morphologies of a cathode and electrolyte through the pores of a GDC layer. The electrical properties of the porous pellets with SSC and YSZ were measured and are shown in Fig. 6. The resistance of SSC and YSZ pellets decreases with increasing temperature.

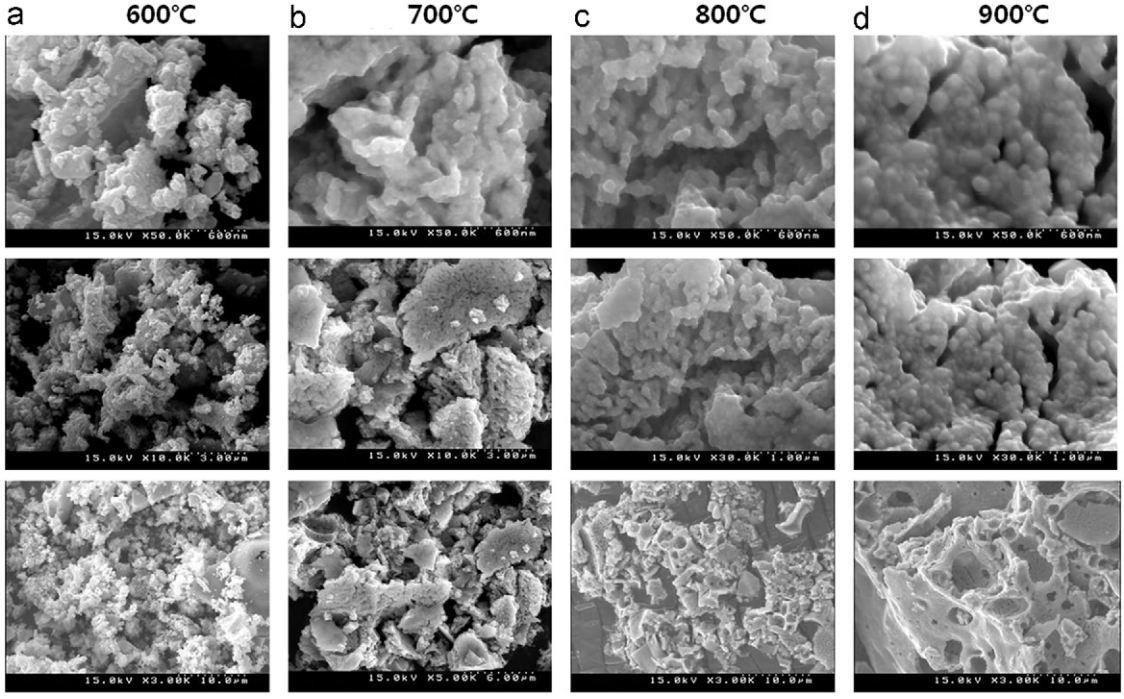

Fig. 3. SEM images of SSC powders calcined at various temperatures.

However, the resistance of the pellets increases at 750 °C due to the formation of second phases, which is coincident with the XRD studies. The second phase peaks appeared in the sample sintered at over 700 °C. The second phase, such as $SrZrO_3$ [25], from the reaction SSC with YSZ, increases the resistance, showing that the second phase is formed by the reaction of SSC with YSZ. After measuring the resistance at 750 °C, the resistances at 700 °C were measured over time. The resistance at 700 °C, after measuring at 750 °C, is higher than before measurement at 750 °C. Resistance increases with time, showing that the reaction is proceeding. The chemical properties and electrical properties of SSC with YSZ show that a barrier layer such as a GDC is crucial for cathode application of SSC in SOFC.

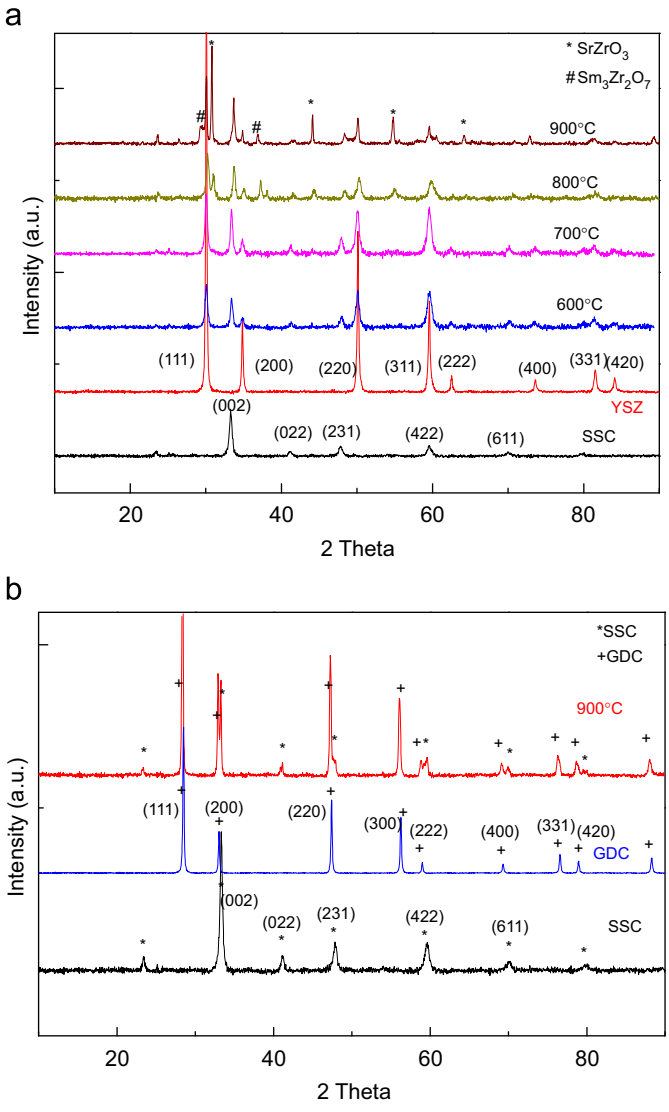

Fig. 4. XRD spectra of composite pellets heat-treated at various temperatures (a) SSC and YSZ and (b) SSC and GDC.

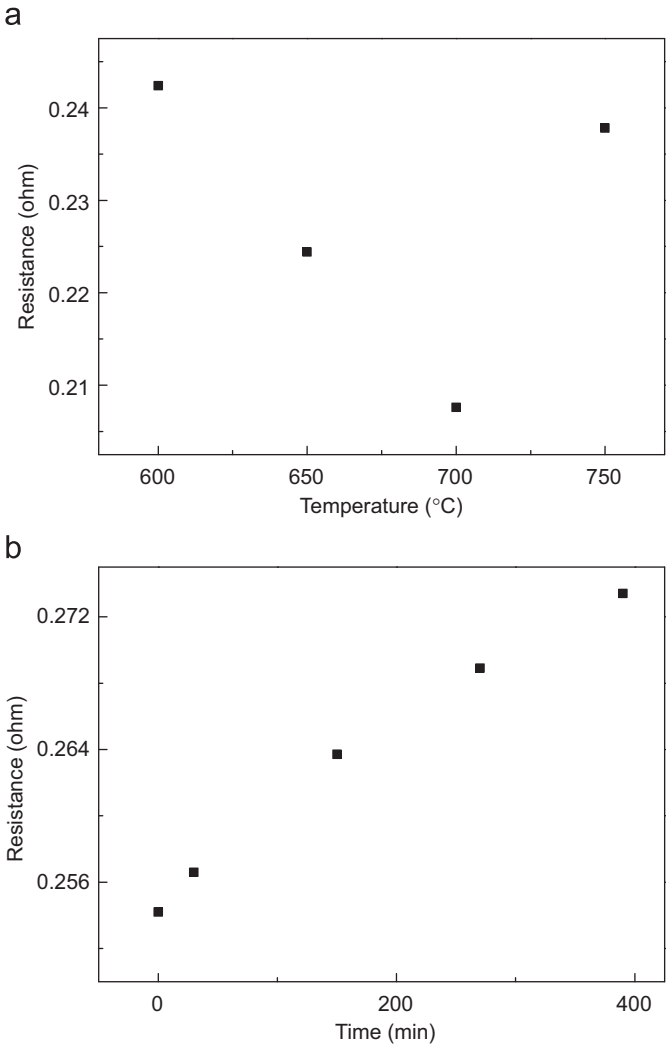

Fig. 6. Electrical Resistance of a porous SSC-YSZ pellet (a) Resistance with temperature and (b) Resistance at 700 °C with time.

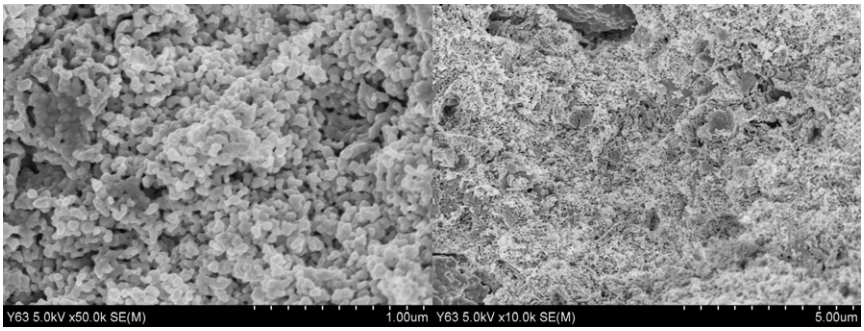

Fig. 5. Morphologies of a porous SSC–YSZ pellet.

The performance of SOFC without a GDC barrier relative to temperature is shown in Fig. 7. Fuel cell performance was measured after reduction of NiO in anode-supported cells with AFL at 580 °C for 3 h. We measured the performance of the fuel cells as temperature increased. SOFCs without a GDC barrier layer show maximum power densities of 0.78 Wcm^{-2}, 0.58 Wcm^{-2}, and 0.4 Wcm^{-2} at 780 °C, 730 °C, and 680 °C, respectively. After measuring the performance of the fuel cells at 780 °C, we measured the performance over time to study the fuel cells' stability. Without a barrier layer, the performance of SOFCs decreases by 23% from 0.78 Wcm^{-2} to 0.6 Wcm^{-2} after 12 h, as shown in Fig. 8 because of the increased resistance from the reaction of SSC with YSZ.

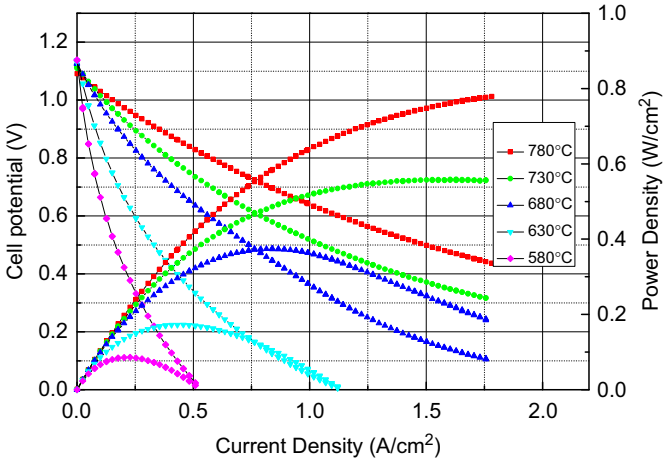

Fig. 7. Fuel Cell Performances of SOFC without a GDC layer.

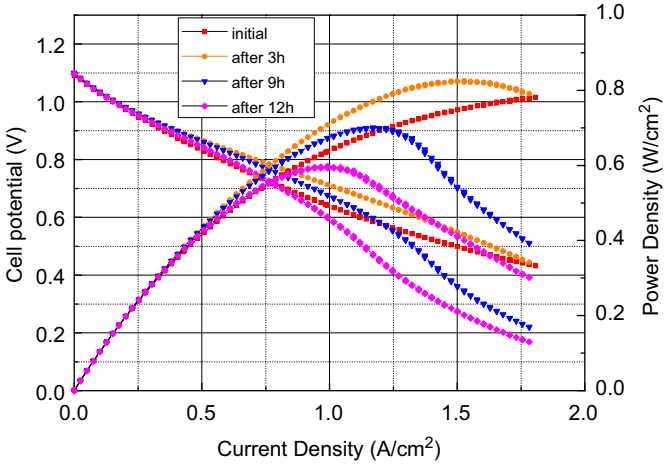

Fig. 8. Fuel cell performances of SOFC without a GDC layer with time at 780 °C.

Images of GDC barrier layers for SOFCs are shown in Fig. 9. The thicknesses of GDC barriers are confirmed and the screen-printed barrier layers are porous as shown in Fig. 9. The fuel cell performance versus thickness of the screen-printed GDC layers is plotted as shown in Fig. 10. SOFCs with a barrier layer show higher performance than those without a GDC layer. SOFCs with a screen-printed GDC barrier show similar values at 780 °C with SOFCs without a barrier layer. However, with decreasing temperature, SOFCs with a thicker barrier layer demonstrate higher values. The performances decrease with decreasing GDC thickness, resulting from the lowered active areas of SSC due to its reaction with YSZ. We expected that a thicker GDC layer would increase ohmic resistance and decrease fuel cell performance. However, SOFCs with a thicker GDC layer show higher fuel cell performance than those with a thinner GDC layer. We expect that there are factors offsetting the increased ohmic resistance. As shown in Fig. 6, the reaction of SSC with YSZ increases the resistance, and when SSC is on a porous GDC layer sintered at 800 °C, the SSC could react with the YSZ through the porous GDC layer. The reactivity of SSC with YSZ through a thin GDC layer is higher. A thicker porous GDC layer increases ohmic resistance, but it also decreases ohmic resistance because of lower reactivity between the SSC and YSZ, more than compensating for the ohmic resistance increase due to a thicker layer. The impedances show the offset effects of the GDC layer, as shown in Fig. 11. The ohmic resistances at 780 °C are similar in SOFCs with and without a screen-printed barrier layer. However, below 730 °C those resistances decrease when the GDC thickness increases, resulting from the lower SSC/YSZ reactivity, again, offsetting the effects of the barrier thickness. Furthermore, as shown in Fig. 11(b), the polarization resistances decrease with increasing barrier thickness because, again, the reactivity is higher through thinner porous GDC layers. The fuel cell performances and impedance spectra show coincident results of the porous GDC layer.

The performance over time of a SOFC with a 5 μm GDC layer is plotted in Fig. 12, which shows that performance decreases by only 3% from 0.75 Wcm^{-2} to 0.72 Wcm^{-2} after 12 h of operation at 780 °C. The degradation of SOFCs with a barrier layer is much lower than that without a barrier layer. The current–voltage characteristics, impedances, and

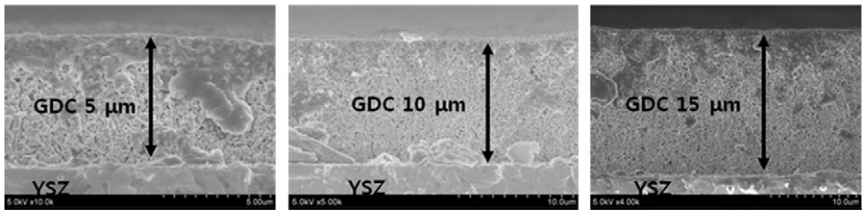

Fig. 9. SEM Images of GDC barriers.

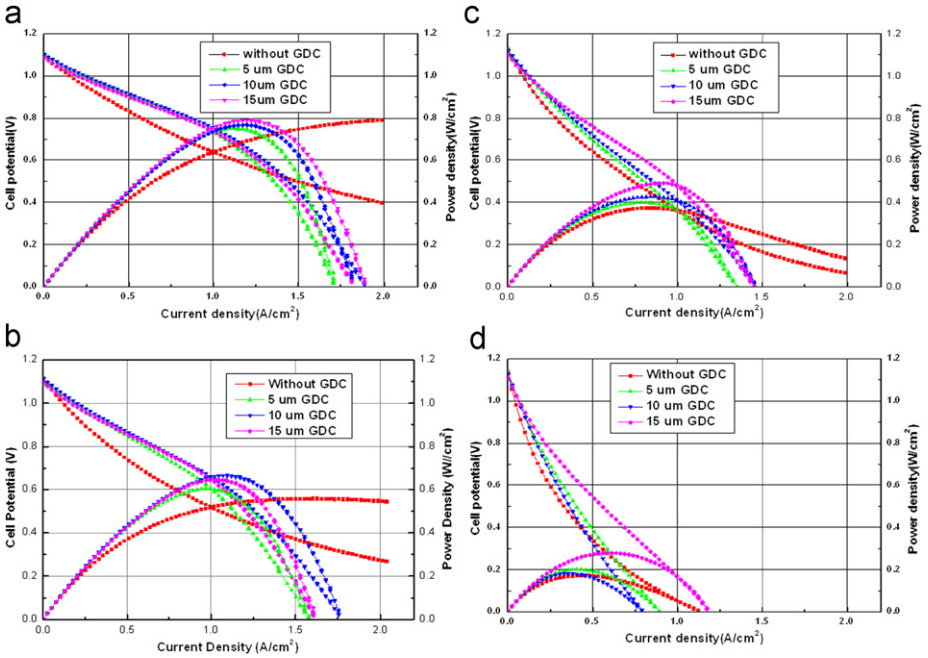

Fig. 10. Fuel Cell Performances of SOFCs with GDC barrier layers at (a) 780 °C, (b) 730 °C (c) 680 °C and (d) 630 °C.

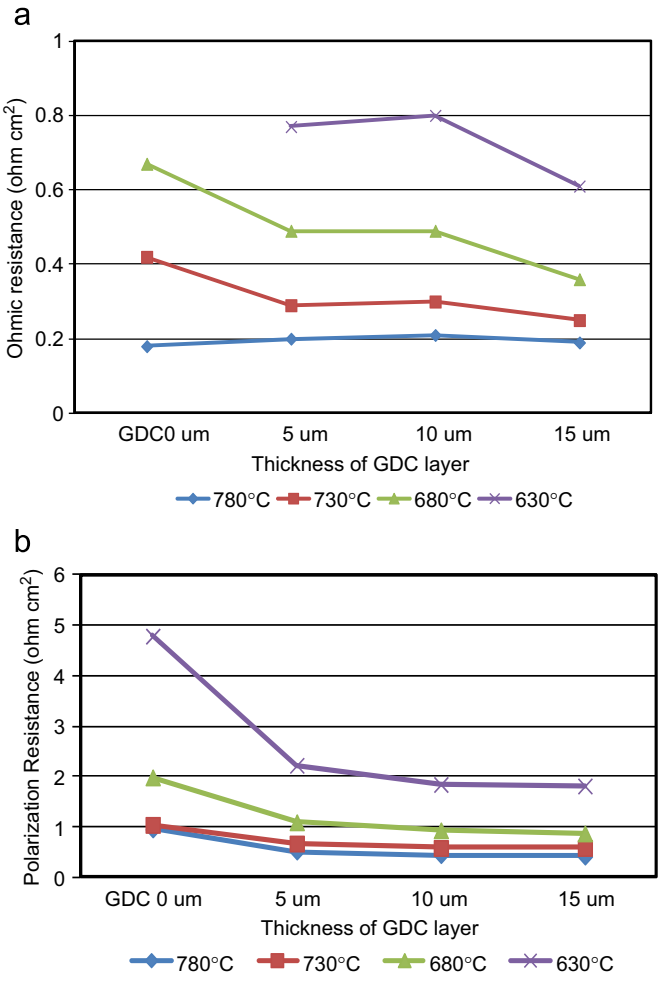

Fig. 11. (a) Ohmic and (b) Polarization resistances of SOFC with the thickness of GDC barrier layer.

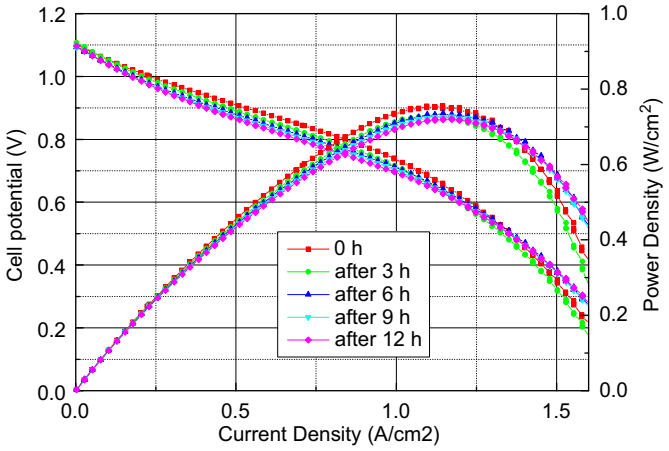

Fig. 12. Fuel Cell Performances of SOFC with 5 μm GDC barrier with time at 780 °C.

performance over time all indicate that a GDC barrier is effective for improving fuel cell performance and stability, and that performance increases with increasing GDC thickness up to 15 μm. In SOFCs with an SSC cathode, a barrier layer of GDC is needed to prevent a reaction of SSC with YSZ.

4. Conclusion

We synthesized nano-structured SSCs with a complex method using citric acid and EDTA. Synthesized SSCs have a calcination temperature of 600 °C, a relatively low temperature, and their particle size calcined at 700 °C is less than 100 nm. SSC reacts with an YSZ electrolyte above 600 °C, which leads to the need for a barrier between the SSC and YSZ. GDC is proposed as a barrier layer. The performance

of SOFCs with a GDC layer increases with increasing thickness of the porous GDC layer. After operation for 12 h at 780 °C, the performance of SOFCs without a barrier layer decreases by 23% from 0.78 Wcm^{-2} to 0.6 Wcm^{-2} and SOFCs with a 5 μm porous GDC layer decrease by only 3% from 0.75 Wcm^{-2} to 0.72 Wcm^{-2}. When SSC is used as a cathode in SOFC, a barrier layer should be applied so as to increase fuel cell performance and stability relative to the thickness of the porous GDC layer.

Acknowledgments

This work was supported by the National Research Foundation (NRF) of Korea Grant funded by the Korean Government (MEST) (NRF-2012–0004203).

References

[1] S.P. Jiang, A comparison of O_2 reduction reactions on porous (La,Sr)MnO_3 and (La,Sr)(Co,Fe)O_3 electrodes, Solid State Ionics 146 (2002) 1–22.

[2] M.J. Jørgensen, M. Mogensen, Impedance of solid oxide fuel cell LSM/YSZ composite cathodes, Journal of the Electrochemical Society 148 (2001) A433–A442.

[3] V. Dusastre, J.A. Kilner, Optimisation of composite cathodes for intermediate temperature SOFC applications, Solid State Ionics 126 (1999) 163–174.

[4] D. Kušščer, J. Holc, S. Hrovat, D. Kolar, Correlation between the defect structure, conductivity and chemical stability of $La_{1-y}Sr_yFe_{1-x}Al_xO_{3-\delta}$ cathodes for SOFC, Journal of the European Ceramic Society 21 (2001) 1817–1820.

[5] A. Mai, V.A.C. Haanappel, S. Uhlenbruck, F. Tietz, D. Stöver, Ferrite-based perovskites as cathode materials for anode-supported solid oxide fuel cells: Part I. Variation of composition, Solid State Ionics 176 (2005) 1341–1350.

[6] A. Mai, V.A.C. Haanappel, S. Uhlenbruck, F. Tietz, D. Stöver, Ferrite-based perovskites as cathode materials for anode-supported solid oxide fuel cells: Part II Influence of the CGO interlayer, Solid State Ionics 177 (2006) 2103–2107.

[7] Y. Teraoka, H.M. Zhang, K. Okamoto, N. Yamazoe, Mixed ionic-electronic conductivity of $La_{1-x}Sr_xCo_{1-y}Fe_yO_{3-\delta}$ perovskite-type oxides, Materials Research bulletin 23 (1988) 51–58.

[8] J. Fleig, On the width of the electrochemically active region in mixed conducting solid oxide fuel cell cathodes, Journal of Power Sources 105 (2002) 228–238.

[9] S.B. Adler, J.A. Lane, B.C.H. Steele, Electrode kinetics of porous mixed-conducting oxygen electrodes, Journal of the Electrochemical Society 143 (1996) 3554–3564.

[10] J.A. Kilner, R.A. De Souza, IC. Fullarton, Surface exchange of oxygen in mixed conducting perovskite oxides, Solid State Ionics 86-88 (1996) 703–709.

[11] J. Fleig, Solid oxide fuel cell cathodes: polarization mechanisms and modeling of the electrochemical performance, Annual Review of Materials Research 33 (2003) 361–382.

[12] X. Zhang, M. Robertson, S. Yick, C. Deĉes-Petit, E. Styles, W. Qu, Y. Xie, R. Hui, J. Roller, O. Kesler, R. Maric, D. Ghosh, $Sm_{0.5}S_{r0.5}CoO_3 + Sm_{0.2}Ce_{0.8}O_{1.9}$ composite cathode for cermet supported thin $Sm_{0.2}Ce_{0.8}O_{1.9}$ electrolyte SOFC operating below 600 °C, Journal of Power Sources 160 (2006) 1211–1216.

[13] S. Yang, T. He, Q. He, $Sm_{0.5}S_{r0.5}CoO_3$ cathode material from glycine-nitrate process: formation, characterization, and application in $LaGaO_3$-based solid oxide fuel cells, Journal of Alloys and Compounds 450 (2008) 400–404.

[14] Y. Guo, H. Shi, R. Ran, Z. Shao, Performance of $SrSc_{0.2}Co_{0.8}O_{3-\delta} + Sm_{0.5}Sr_{0.5}CoO_{3-\delta}$ mixed-conducting composite electrodes for oxygen reduction at intermediate temperatures, The International Journal of Hydrogen Energy 34 (2009) 9496–9504.

[15] W. Zhou, Z. Shao, R. Ran, R. Cai, Novel $SrSc_{0.2}Co_{0.8}O_{3-\delta}$ as a cathode material for low temperature solid-oxide fuel cell, Electronics and Communications 10 (2008) 1647–1651.

[16] Y.L. Yang, C.L. Chen, S.Y. Chen, C.W. Chu, A.J. Jacobson, Impedance studies of oxygen exchange on dense thin film electrodes of $La_{0.5}Sr_{0.5}CoO_3$ – delta, Journal of the Electrochemical Society 147 (2000) 4001–4007.

[17] Y. Liu, W. Rauch, S. Zha, M. Liu, Fabrication of $Sm_{0.5}Sr_{0.5}CoO_{3-\delta}$ – $Sm_{0.1}Ce_{0.9}O_{2-\delta}$ cathodes for solid oxide fuel cells using combustion CVD, Solid State Ionics 166 (2004) 261–268.

[18] E.P. Murray, M.J. Sever, S.A. Barnett, Electrochemical performance of (La,Sr)(Co,Fe)O_3–(Ce,Gd)O_3 composite cathodes, Solid State Ionics 148 (2002) 27–34.

[19] Z. Shao, S.M. Haile, A high-performance cathode for the next generation of solid-oxide fuel cells, Nature 431 (2004) 170–173.

[20] Z. Shao, W. Yang, Y. Cong, H. Dong, J. Tong, G. Xiong, Investigation of the permeation behavior and stability of a $Ba_{0.5}Sr_{0.5}Co_{0.8}Fe_{0.2}O_{3-\delta}$ oxygen membrane, Journal of Membrane Science 172 (2000) 177–188.

[21] Q. Zhu, T. Jin, Y. Wang, Thermal expansion behavior and chemical compatibility of $Ba_xSr_{1-x}Co_{1-y}Fe_yO_{3-\delta}$ with 8YSZ and 20GDC, Solid State Ionics 177 (2006) 1199–1204.

[22] S.B. Adler, Limitations of charge-transfer models for mixed-conducting oxygen electrodes, Solid State Ionics 135 (2000) 603–612.

[23] A. Petric, P.H.F. Tietz, Evaluation of La–Sr–Co–Fe–O perovskites for solid oxide fuel cells and gas separation membranes, Solid State Ionics 135 (2000) 719–725.

[24] H. Fukunaga, M. Koyama, N. Takahashi, C. Wen, K. Yamada, Reaction model of dense $Sm_{0.5}Sr_{0.5}CoO_3$ as SOFC cathode, Solid State Ionics 132 (2000) 279–285.

[25] H.Y. Tu, Y. Takeda, N. Imanishi, O. Yamamoto, $Ln_{1-x}Sr_xCoO_3$(Ln=Sm, Dy) for the electrode of solid oxide fuel cells, Solid State Ionics 100 (1997) 283–288.

[26] W. Zhu, Z. Lu, S. Li, B. Wei, J. Miao, X. Huang, K. Chen, N. Ai, W. Su, Study on $Ba_{0.5}Sr_{0.5}Co_{0.8}Fe_{0.2}O_{3-\delta}$ – $Sm_{0.5}Sr_{0.5}CoO_{3-\delta}$ composite cathode materials for IT-SOFCs, Journal of Alloy and Compounds 465 (2008) 274–279.

[27] F.S. Baumann, J. Maier, J. Fleig, The polarization resistance of mixed conducting SOFC cathodes: a comparative study using thin film model electrodes, Solid State Ionics 179 (2008) 1198–1204.

[28] T. Ishihara, M. Honda, T. Shibayama, H. Minami, H. Nishiguchi, V. Takita, Intermediate temperature solid oxide fuel cells using a new $LaGaO_3$ based oxide ion conductor, Journal of the Electrochemical Society 145 (1998) 3177–3183.

[29] H. Jung, Y. Sun, H. Jung, J. Park, H. Kim, G. Kim, H. Lee, J. Lee, Investigation of anode-supported SOFC with cobalt-containing cathode and GDC interlayer, Solid State Ionics 179 (2008) 1535–1539.

[30] T. Suzuki, B. Liang, T. Yamaguchi, H. Sumi, K. Hamamoto, Y. Fujishiro, One-step sintering process of gadolinia-doped ceria interlayer–scandia-stabilized zirconia electrolyte for anode supported microtubular solid oxide fuel cells, Journal of Power Sources 199 (2012) 170–173.

[31] D. Yang, X. Zhang, S. Nikumb, C. Deces-Petit, R. Hui, R. Maric, D. Ghosh, Low temperature solid oxide fuel cells with pulsed laser deposited bi-layer electrolyte, Journal of Power Sources 164 (2007) 182–188.

[32] X. Zhang, M. Robertson, C. Deces-Petit, Y. Xie, R. Hui, W. Qu, O. Kesler, R. Maric, D. Ghosh, Solid oxide fuel cells with bi-layered electrolyte structure, Journal of Power Sources 175 (2008) 800–805.

[33] V.V. Srdic, R.P. Omorjan, J. Seidel, Electrochemical performances of $(La,Sr)CoO_3$ cathode for zirconia-based solid oxide fuel cells, Materials Science and Engineering B 116 (2005) 119–124.